

DESIGN OF A TWO-STAGE OVEN SOURCE TO DETERMINE THE ENTHALPY
OF INTERCONVERSION OF THE LOWEST ENERGY CONFORMERS OF N-
ACETYL-GLYCINE-METHYLAMIDE (NAGMA)

by

CAITLYNE CELESTE SHIRLEY

(Under the Direction of Gary E. Douberly)

ABSTRACT

Modeling the gas-phase energetics of biomolecules is challenging because of their low vapor pressure and the presence of many low energy conformations. However, helium nanodroplet isolation (HENDI) techniques can trap and cool vibrationally hot model biomolecules in an environment with negligible solvent effects. Sufficiently high-resolution vibrational spectra obtained for biomolecules in this environment allows for the separation of bands due to different conformations. Enthalpies of interconversion between conformers can therefore be determined from a van't Hoff analysis of the temperature dependence of vibrational bands in the infrared spectrum. In this study, a two-stage oven source was designed to introduce a constant vapor pressure of the model biomolecule N-acetyl-glycine-methylamide (NAGMA) into the gas phase. Its infrared spectrum was probed at various temperatures in order to determine the temperature dependence of the equilibrium constant associated with the interconversion of two low energy conformers. The first oven was kept at a fixed temperature to ensure that a constant number density of NAGMA was introduced into a second variable temperature oven source. From this data, the equilibrium constant was determined as a function of

temperature and a van't Hoff plot was generated to determine the enthalpy of conformer interconversion. The $\Delta H^\circ_{c5 \leftrightarrow c7} = -4.52 \pm 0.12 \text{ kJ/mol}$.

INDEX WORDS: NAGMA, gas-phase, equilibrium constant, van't Hoff, HENDI, infrared spectroscopy, enthalpy, conformer, interconversion

DESIGN OF A TWO-STAGE OVEN SOURCE TO DETERMINE THE ENTHALPIES
OF INTERCONVERSION OF THE LOWEST ENERGY CONFORMERS OF N-
ACETYL-GLYCINE-METHYLAMIDE (NAGMA)

by

CAITLYNE CELESTE SHIRLEY

BS, University of Southern Mississippi, 2011

A Thesis Submitted to the Graduate Faculty of The University of Georgia in Partial
Fulfillment of the Requirements for the Degree

MASTER OF SCIENCE

ATHENS, GEORGIA

2014

© 2014

Caitlyne Celeste Shirley

All Rights Reserved

DESIGN OF A TWO-STAGE OVEN SOURCE TO DETERMINE THE ENTHALPIES
OF INTERCONVERSION OF THE LOWEST ENERGY CONFORMERS OF N-
ACETYL-GLYCINE-METHYLAMIDE (NAGMA)

by

CAITLYNE CELESTE SHIRLEY

Major Professor: Gary E. Douberly

Committee: Michael A. Duncan
Geoffrey D. Smith

Electronic Version Approved:

Maureen Grasso
Dean of the Graduate School
The University of Georgia
May 2014

ACKNOWLEDGEMENTS

I would first like to acknowledge my principal investigator, Dr. Gary Douberly, for accepting me into his lab to develop my skills and understanding of experimental physical chemistry. Without his expert guidance, this research project would not be possible. I would also like to thank my colleagues Chris Moradi, Tao Liang, Emmanuel Obi, Brad Acrey, Joe Brice, Alex Morrison, Steven Flynn, and Paul Raston. I would especially like to thank Grant Moody for his preliminary work on the NAGMA project, including his help on the survey scan, the OSMS, and early calculations. And lastly, I owe a great debt of gratitude to Chris Leavitt. From the multitude of calculations he contributed to this project as well as the long hours he spent with me tweaking the experimental design and gathering the spectra necessary to determine the enthalpy of interconversion of NAGMA, I cannot thank him enough. Without his help the completion of this experiment would have been a much more arduous task.

While building the two-stage oven source I had the pleasure of working with many wonderful people in various departments of UGA. I would like to thank Richard Harrison in the glass blowing studio for his swift work creating the two nested round-bottom flask sample container for the early design of the first stage of the oven source. I would like to thank the UGA Instrument Design and Fabrication Shop for turning my designs for the aluminum block and its pipe connector for the second stage of the oven source into a reality. I would also like to thank the National Science Foundation (Grant No. CHE-1054742) for funding this project.

Last but not least, I would like to thank my partner, Anthony Kyle English, for helping me through this process. He has been a constant source of comfort during my time at UGA. With him I celebrated triumphs and shared disappointments. Throughout all of this, he has provided constant support, sympathy, and most importantly, his love. I cannot thank him enough for that.

TABLE OF CONTENTS

	Page
ACKNOWLEDGEMENTS	iv
LIST OF FIGURES	viii
CHAPTER	
1 THE ENERGETICS OF BIOMOLECULES	1
1.1 Purpose of study.....	1
1.2 Energetics of conformers	2
1.3 Trapping of conformers in low temperature helium	7
1.4 Probing N-H stretches via IR spectroscopy	9
2 DESIGN OF A TWO-STAGE OVEN SOURCE FOR PICKUP OF NAGMA BY HELIUM NANODROPLETS FOR IR LASER INTERROGATION.....	12
2.1 Two-stage oven source design	12
2.2 Evolution of the design of a two-stage oven source	14
2.3 NI LabVIEW™ temperature stabilization program	19
2.4 Mass spectrometer detection.....	20
2.5 Infrared laser interrogation of conformer distributions in helium nanodroplets.....	23
3 THE ENTHALPY OF INTERCONVERSION OF NAGMA.....	26
3.1 Mass spectra of NAGMA	26
3.2 Infrared spectroscopy of NAGMA	28
3.3 Assignments of the two conformers of NAGMA to spectra.....	29

3.4 Enthalpy of interconversion from the van't Hoff plot	32
4 CONCLUSIONS AND FUTURE PROJECTS	35
REFERENCES	37

LIST OF FIGURES

	Page
Figure 1.1: N-acetyl-glycine-methylamide	2
Figure 1.2: The C5 conformer of NAGMA	4
Figure 1.3: The C7 conformer of NAGMA	4
Figure 1.4: The C5 and C7 conformers of NAGMA	5
Figure 1.5: A general van't Hoff plot	7
Figure 1.6: The effect of temperature on rovibrational spectra	8
Figure 1.7: The electric field polarization dependence of signal intensity (blue dotted line represents the helium droplet beam)	11
Figure 2.1: The first stage oven source	13
Figure 2.2: The second stage oven source	14
Figure 2.3: View of the front and back faces of the aluminum block	16
Figure 2.4: Lengthwise views of the aluminum block	17
Figure 2.5: Biomolecule source	18
Figure 2.6: The HENDI experimental design	20
Figure 2.7: The HENDI setup including the Stark cell	21
Figure 2.8: Neat helium droplet mass spectrum	22
Figure 2.9: Experimental setup of the cw-SR-OPO coupled to a HENDI spectrometer ..	24
Figure 3.1: The mass spectrum of NAGMA scanned from $m/z = 10-75$	26
Figure 3.2: OSMS of N-H stretches studied	27
Figure 3.3: Survey scan of NAGMA	28

Figure 3.4: A blown up view of the N-H nonbonded stretches of the C5 and C7 conformers	29
Figure 3.5: The experimental and calculated VTMA's at the MP2/def2-TZVPD level of theory for the C5 conformer. The solid line corresponds to the simulation using the computed VTMA for the free N-H stretch of the C5 conformer, namely 70°.	31
Figure 3.6: The experimental and calculated VTMA's at the MP2/def2-TZVPD level of theory for the C7 conformer. The solid line corresponds to the simulation using the computed VTMA for the free N-H stretch of the C7 conformer, namely 78°.	32
Figure 3.7: The van't Hoff plot of the interconversion of C5↔C7	33
Figure 3.8: DFT and ab initio calculations of the enthalpy of interconversion of NAGMA (C5↔C7).....	34

CHAPTER 1

THE ENERGETICS OF BIOMOLECULES

1.1 Purpose of study

The structure-function relationship of biomolecules is a complex and intriguing area of study in the bio-physical sciences. Diseases such as Alzheimer, Creutzfeldt-Jakob, arthritis, diabetes, and many more are caused by misfolded proteins (prions). The thermodynamics of protein misfolding are integral to our understanding of how prions are formed and how they interact with other proteins and substrates. As pointed out by Jäger, et al.,¹ globular proteins evolve partially through selection, the criteria of which are what function the protein serves and the thermodynamic stability to avoid chaperone binding and degradation by scavenging proteases. The current theoretical methods that are used to determine the thermodynamic properties of proteins and amino acids are incomplete, and in some cases, completely nonexistent.^{2,3} In the past few years, great strides have been made in theoretical and computational chemistry to predict various physical properties of biomolecules.^{2,4-7} However, the current methods capable of accurately predicting enthalpies of interconversion between different conformers are too expensive to be applied generally. The secondary structure of proteins is difficult to probe directly with infrared spectroscopy as the massive amount of infrared active stretches that exist complicate the vibrational spectra of even the most basic complete protein. For example, Brauner, et al., stated that there is much to be improved upon structure-frequency correlations, that subbands from helices, sheets, turns, and loops are broader and overlap

more than is currently used in theory, and that the traditional α -helical marker band is sometimes distorted in short segments.⁸ However, by probing the spectra of model dipeptides, it is then possible to probe both the signatures of various structural motifs and the local gas-phase energetics of a protein building block. The model dipeptide used in this study is N-acetyl-glycine-methylamide (NAGMA), seen in Figure 1.1.

The high temperature required to increase the vapor pressure of N-acetyl-glycine-methylamide (NAGMA) sufficiently for it to enter the gas phase contributes to the complexity of its infrared spectrum because of broad rotational contours. In order to simplify the IR spectrum associated with the gas phase equilibrium conformer distribution, the high-temperature gas-phase NAGMA sample is entrained in helium droplets and cooled to 0.37 K. Infrared bands of the lower-energy conformers are assigned on the basis of a vibrational transition moment angle (VTMA) analysis.

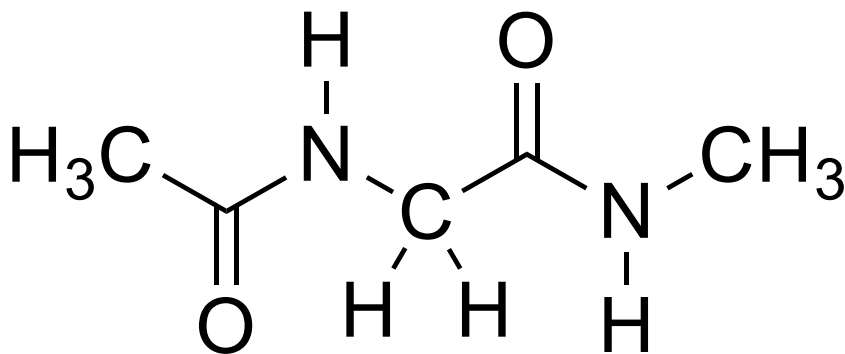


Figure 1.1: N-acetyl-glycine-methylamide

1.2 Energetics of conformers

Out of the numerous studies of the structural and conformational preferences of model dipeptides,⁹⁻¹⁴ there are almost none that discuss the energetics of model dipeptides. Previous studies of the energetics of the conformers of peptides have dealt with peptides chelated with cations.^{15,16} There are also studies that involve the enthalpies of formation^{2,17,18} and structural dynamics of RNA and peptides,^{1,19-22} but relatively few

that address the gas phase enthalpies of interconversion of bare, model dipeptides.²³

NAGMA has two low energy conformers, C5 and C7, shown below in their MP2/aug-cc-pVTZ optimized geometries in Figures 1.2 and 1.3. No other conformers were found within 10 kcal/mol of these two at this level of theory.

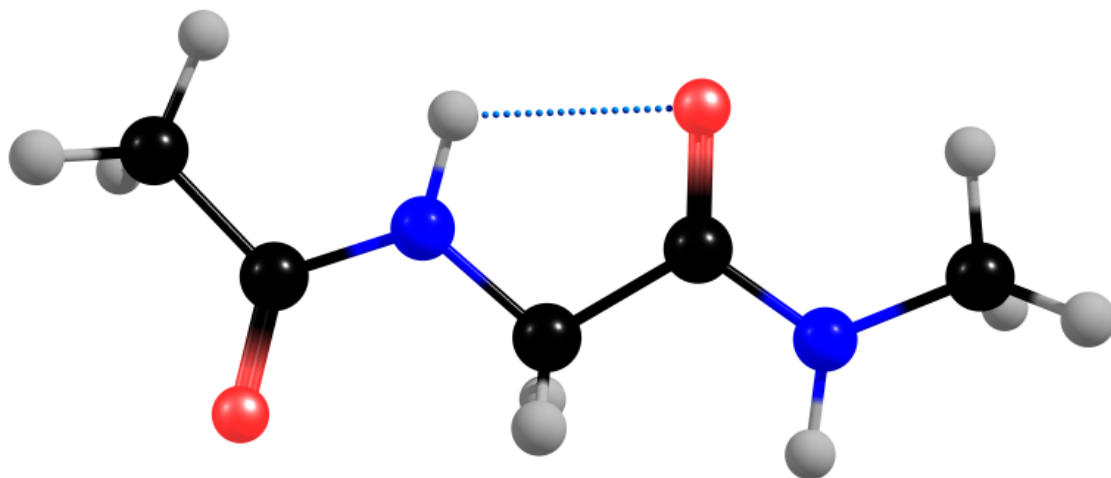


Figure 1.2: The C5 conformer of NAGMA

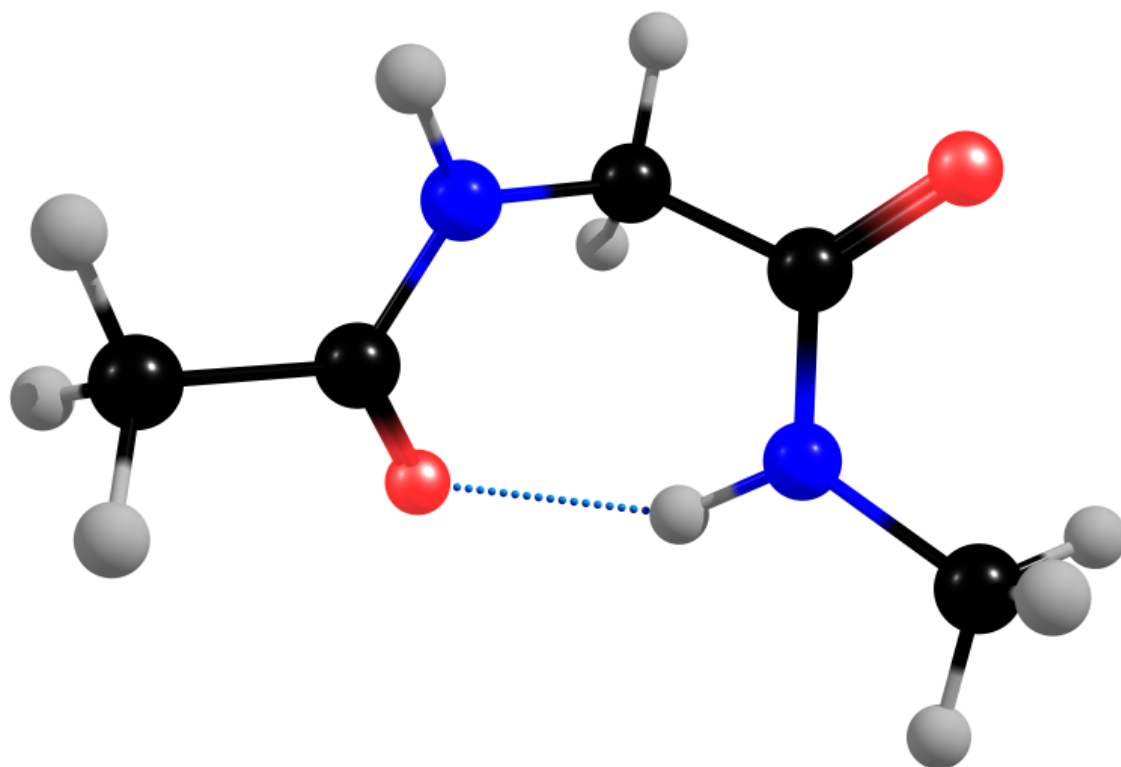


Figure 1.3: The C7 conformer of NAGMA

The naming scheme of the conformers is derived from the hydrogen-bonding structures in which they are most stable. The C5 and C7 conformers are stabilized by

hydrogen bonds between the C=O and N-H groups to form either a five- or seven-membered ring. The hydrogen-bonding scheme without geometry optimization is shown below in Figure 1.4. The cartoon below demonstrates the bonding between different C=O and N-H groups to form the five-membered ring in conformer C5 and the seven-membered ring in conformer C7.

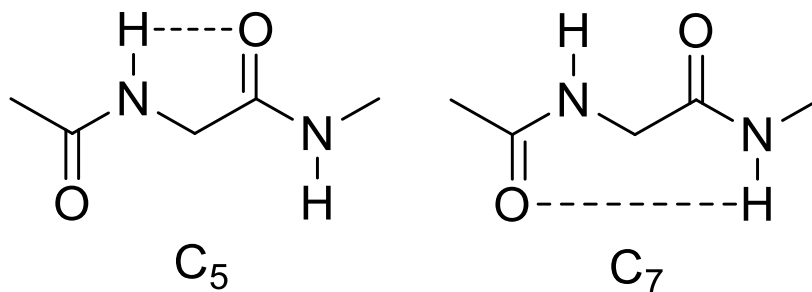


Figure 1.4: The C5 and C7 conformers of NAGMA

In this study, the enthalpy of interconversion of two low-energy conformers is determined by van't Hoff analysis. Potts and Baer²⁴ have demonstrated how to experimentally determine the enthalpy of interconversion of two conformers using a van't Hoff analysis. In order to determine the enthalpy of interconversion for these two low energy conformers, a van't Hoff analysis was carried out in which the equilibrium constants associated with the interconversion of these conformations was monitored at various temperatures. The van't Hoff equation is shown below.

$$\ln K_{eq} = -\frac{\Delta H^{\ominus}}{RT} + \frac{\Delta S^{\ominus}}{R}$$

Even though enthalpy is temperature dependent, this effect is assumed to be negligible over a small temperature range. By taking a linear regression of $\ln K_{eq}$ vs. T^{-1} , the enthalpy of interconversion can be determined where $y = \ln K_{eq}$, $m = -\frac{\Delta H^{\ominus}}{RT}$, and $b = \frac{\Delta S^{\ominus}}{R}$. In this experiment, the equilibrium constant is determined from the relative

intensities of N-H stretch bands in the infrared spectrum. $K_{eq} = \frac{C7t^2_{C5}}{C5t^2_{C7}}$, where t_x is the transition dipole moment for the free N-H stretch, and C7 and C5 are the integrated areas of these N-H stretch bands for either the C7 or C5 conformer, respectively. The C7 and C5 values were determined from Lorentzian lineshape fits to the observed N-H stretch bands in the 3490-3500 cm^{-1} region. The transition dipole moments are not temperature dependent, and so they cancel out upon differentiation of $\ln K_{eq}$ with respect to $1/T$, as shown below.

$$\frac{d \ln K_{eq}}{d\left(\frac{1}{T}\right)} = \frac{-\Delta H}{R}$$

$$\ln K_{eq} = \ln \frac{C7}{C5} + \ln \frac{t^2_{C5}}{t^2_{C7}}$$

$$\frac{d \ln K_{eq}}{d\left(\frac{1}{T}\right)} = \frac{d \ln \left(\frac{C7}{C5}\right)}{d\left(\frac{1}{T}\right)} + 0 = -\frac{\Delta H}{R}$$

Hence, $\frac{d \ln \left(\frac{C7}{C5}\right)}{d\left(\frac{1}{T}\right)} = -\frac{\Delta H^\ominus}{R}$ and the linear equation is $\ln \left(\frac{C7}{C5}\right) = -\frac{\Delta H}{RT} + \frac{\Delta S}{R} - \ln \left(\frac{t^2_{C5}}{t^2_{C7}}\right)$.

Therefore, a van't Hoff plot setting $\ln \frac{C7}{C5}$ as the y-coordinate and $\frac{1}{T}$ as the x-coordinate

yields a slope with the value $-\frac{\Delta H}{R}$ and an intercept equal to $b = \frac{\Delta S^\ominus}{R} - \ln \left(\frac{t^2_{C5}}{t^2_{C7}}\right)$. An

example of a van't Hoff plot is shown below in Figure 1.5.

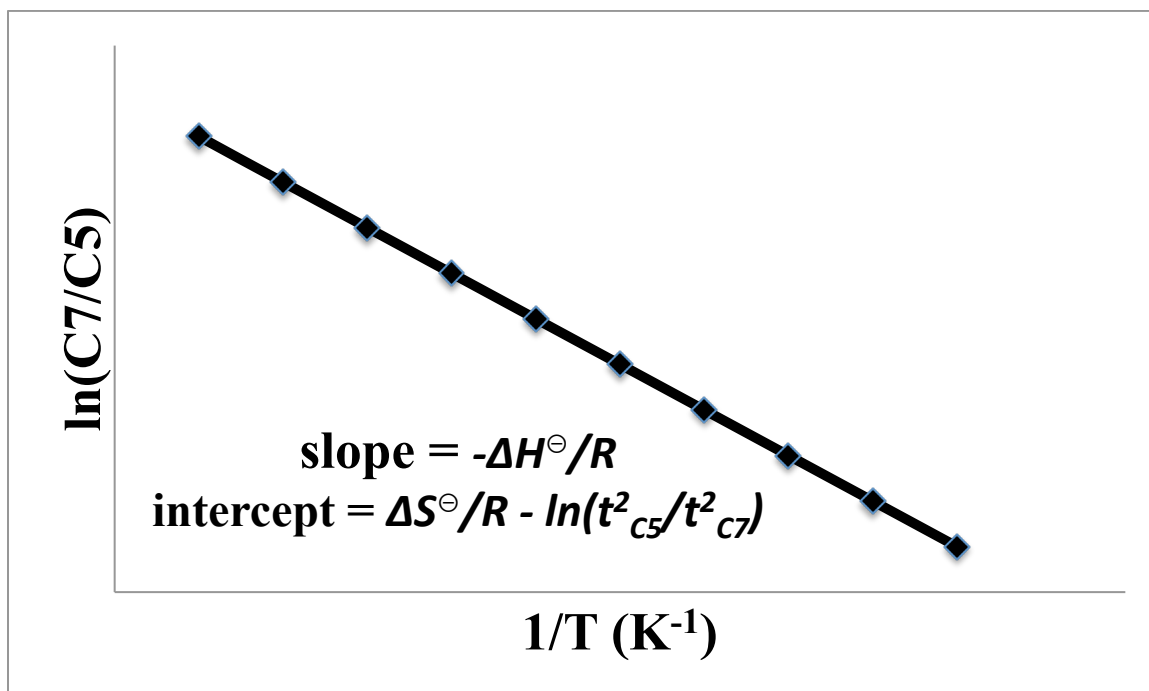


Figure 1.5: A general van't Hoff plot

1.3 Trapping of conformers in low temperature He

High temperature spectra suffer from poor resolution. At higher temperatures there are more populated rotational states, and therefore there is lower line intensity for the lowest lying rotational states.²⁵ The “rotational envelope” sharpens at lower temperatures and broadens at higher temperatures, as shown below in Figure 1.6.²⁵ Broadening is also attributed to molecular motions and collisions, which are more numerous and energetic at higher temperatures.

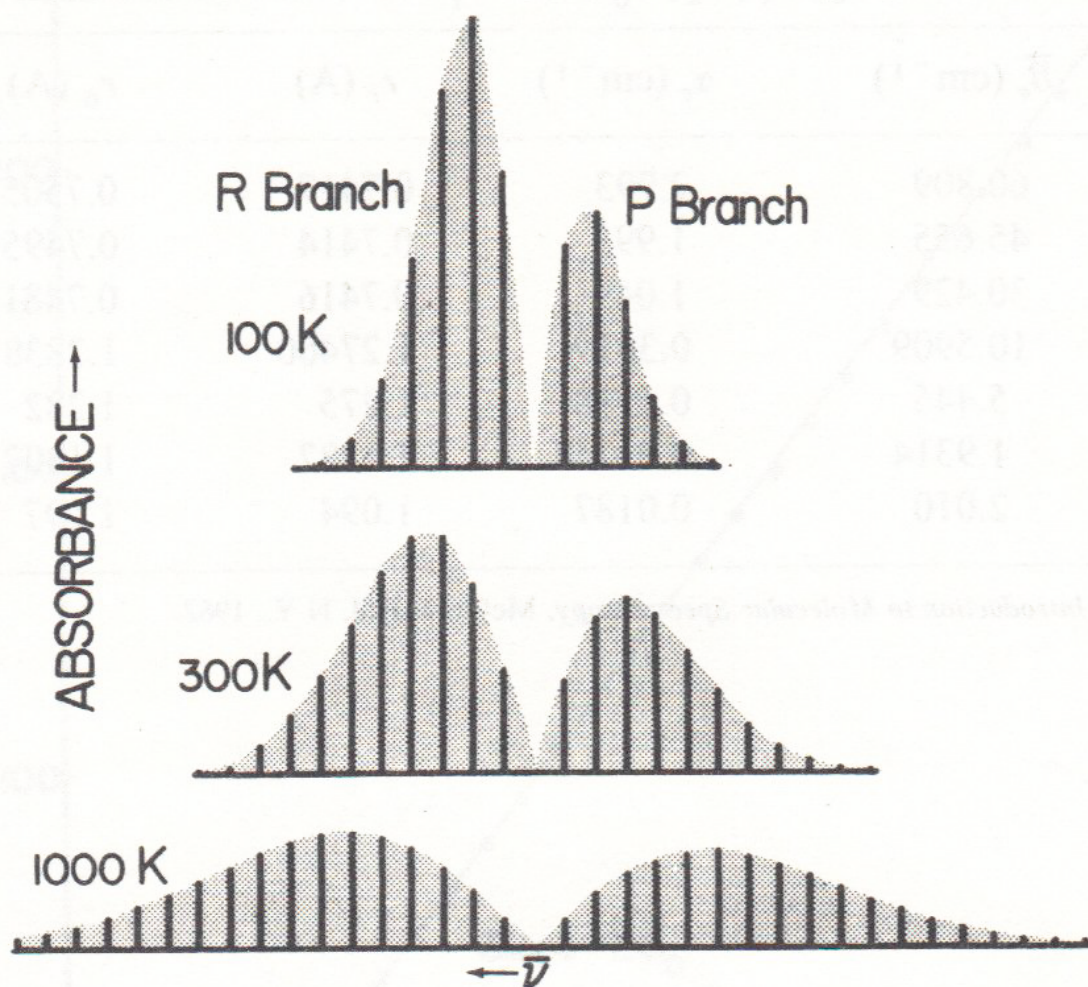


Figure 1.6: The effect of temperature on rovibrational spectra²⁵

The HENDI technique is used in order to simplify the spectrum of the vibrationally hot NAGMA. Helium nanodroplets are formed under high pressure (30 bar) behind a 5 μm nozzle cooled to low temperatures (~ 18 K). Under these free-jet expansion conditions, the droplets cool from 14-24 K to 0.37 K (for ^4He clusters). However, molecules of NAGMA are solvated into the helium nanodroplets at the temperature of the pick-up cell, ranging from ~ 400 -670 K. Again, the droplets cool to 0.37 K by evaporation of helium atoms. In order to determine the conformer distribution at the temperature of the oven source, the rate of isomerization must be less than the rate of

vibrational relaxation upon helium solvation.²⁴ It has been shown that evaporative cooling removes internal energy at a rate at least on the order of 10^{12} K/s.²⁶ We can deduce that this is most likely true here, because at the droplet temperature only the lowest energy conformer of NAGMA would be populated at equilibrium, whereas multiple conformers are observed spectroscopically. This observation suggests that the vibrational cooling rate is sufficiently rapid to preserve the oven temperature NAGMA population distribution upon helium solvation.²⁷ Throughout, we assume the conformer distribution of NAGMA is representative of the distribution at the oven source temperature.

1.4 Probing N-H stretches via IR spectroscopy

Each doped helium nanodroplet contains around 10^4 helium atoms per solvated NAGMA molecule. Therefore, the detection technique used to determine the infrared spectrum of the biomolecule must be quite sensitive. Upon vibrational excitation of NAGMA, vibrational energy is transferred to the helium nanodroplet.²⁸ Because of the small energy barrier to evaporation, the droplet loses hundreds of helium atoms, which is detected as a decrease in the ion signal by a quadrupole mass spectrometer. Electron impact ionizes a helium atom, and subsequent charge hopping occurs leading to the formation of either He_n^+ or charge transfer to NAGMA. Because there is about a 14 eV difference in ionization potential between helium and NAGMA, the energy imparted to the nanodroplet causes desolvation and fragmentation of NAGMA upon charge transfer. In our experiment, mass channel $m/z = 30$ was monitored, which corresponds to the CH_3NH^+ fragment. As the infrared laser comes into resonance with a NAGMA transition, evaporation occurs which decreases the ionization cross-section of the droplet.

In this experiment, the laser induced depletion signal corresponds to the reduction of ion current for the CH_3NH^+ fragment in the mass spectrometer. The ion signal depletion is 100-1000 times larger than the noise when processed with a lock-in amplifier, making this technique sensitive enough to measure the vibrational spectrum of NAGMA.

In order to determine the conformer that corresponds to a specific vibrational band, the technique of polarization spectroscopy is used to determine the vibrational transition moment angle (VTMA) associated with each transition,²⁹ which is then compared to ab initio theoretical predictions. The angle between the permanent dipole moment and a specific transition dipole moment is called the vibrational transition moment angle (VTMA). The transition dipole moment vector points roughly in the direction of the stretch that is probed. Any molecule with a permanent dipole moment can be oriented in a dc electric field along the dipole moment direction. For rotationally cold molecules, such as those in a helium nanodroplet, the dc electric fields necessary for strong lab-frame orientation are modest (<50 kV/cm). For a molecule with a permanent dipole moment parallel to its transition dipole moment (parallel band), a corresponding enhancement in signal appears if the laser is polarized parallel to the dc electric field. Likewise, there is a corresponding decrease in signal intensity with a perpendicularly polarized laser, as shown in Figure 1.7.

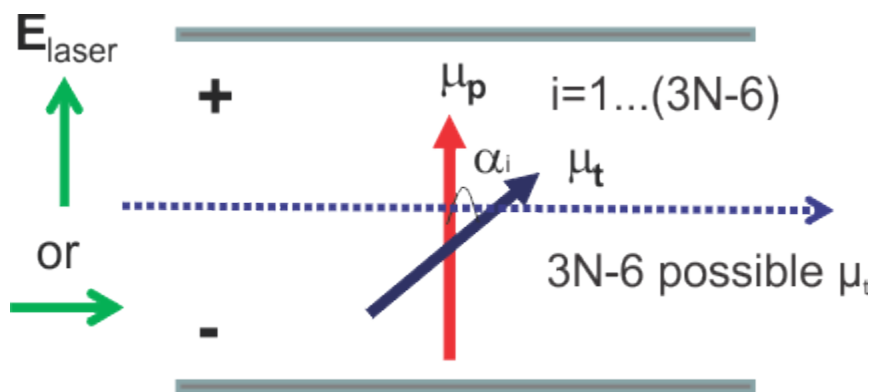


Figure 1.7: The electric field polarization dependence of signal intensity (blue dotted line represents the helium droplet beam)

In the above figure, α_i is the vibrational transition moment angle for a certain vibrational mode of a molecule [$i=1 \dots (3N-6)$] between the permanent dipole moment μ_p and the transition moment dipole μ_t . In our case, the modes of interest are the N-H stretches of NAGMA, two for each low-energy conformation. To determine the VTMA, the helium-solvated molecules are aligned in the laboratory frame along their permanent dipole moments. By comparing the experimentally determined VTMA with *ab initio* calculations, the experimentally measured vibrational bands can be assigned definitively to a specific conformer, because the computed VTMA are shown to be strongly conformer dependent. Because any non-linear molecule, such as NAGMA, has $3N-6$ vibrational modes, there is a wealth of structural information that can be gleaned from VTMA. See Miller, et al,²⁸ for a more detailed discussion of the mathematics involved with determining VTMA.

CHAPTER 2

DESIGN OF A TWO-STAGE OVEN SOURCE FOR PICKUP OF NAGMA BY HELIUM NANODROPLETS FOR IR LASER INTERROGATION

2.1 Two-stage oven source design

If the vapor pressure of NAGMA is too large, the helium nanodroplets will pick up multiple molecules with high probability. If two NAGMA dipeptides are picked up by a helium nanodroplet, a dimer is formed; if three, a trimer, etc. The temperatures at which NAGMA is studied in order to generate the van't Hoff plot would create a vapor pressure of NAGMA far greater than the optimum vapor pressure for monomer pickup of the dipeptide. In order to keep a constant vapor pressure of NAGMA, optimized for monomer pickup, while still varying the temperature at which the conformer distributions are frozen, a two-stage oven source was designed. The first oven resides outside of the vacuum chamber and consists of a Swagelok™ cap that is filled with NAGMA. Figure 2.1 below shows the first stage oven source including vacuum feedthroughs for all variable transformers, the dc power source, and thermocouple wires. It is connected to a stainless steel pipe that enters the vacuum chamber using a copper gasketed Swagelok™ pipe feedthrough. Both the Swagelok™ cap and the atmosphere side of the pipe are heated using heat wrap tape controlled with a variable transformer. The stainless steel pipe connects to the second stage oven, shown in Figure 2.2. This oven is an aluminum block heated with one large cartridge heater and two small cartridge heaters. The two small cartridge heaters are connected in series. The

large cartridge heater connects to a variable transformer for rough temperature adjustment, and the small cartridge heaters are connected to a dc power source (GW Instek PST-3202) for fine adjustment. To avoid NAGMA condensation inside the transfer pipe between stages one and two, an insulated nichrome wire is wrapped around the pipe and resistively heated inside the vacuum chamber.

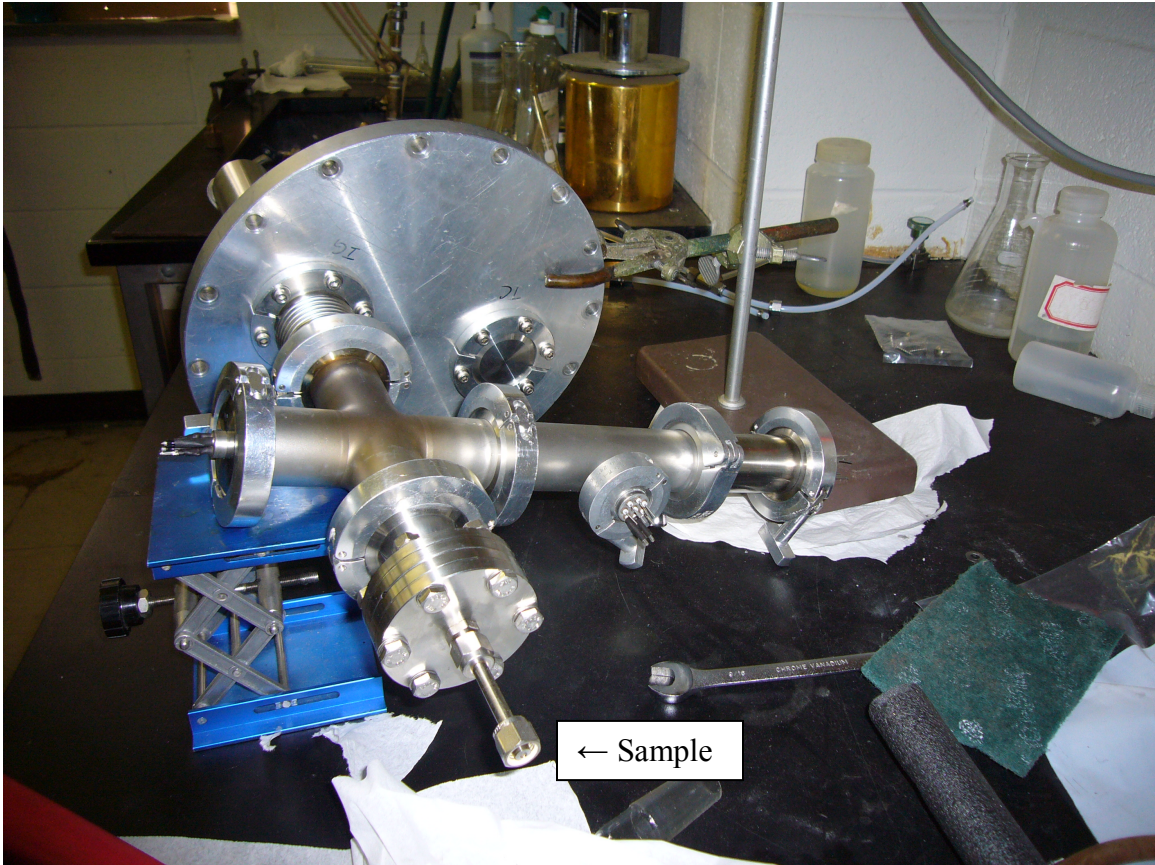


Figure 2.1: The first stage oven source

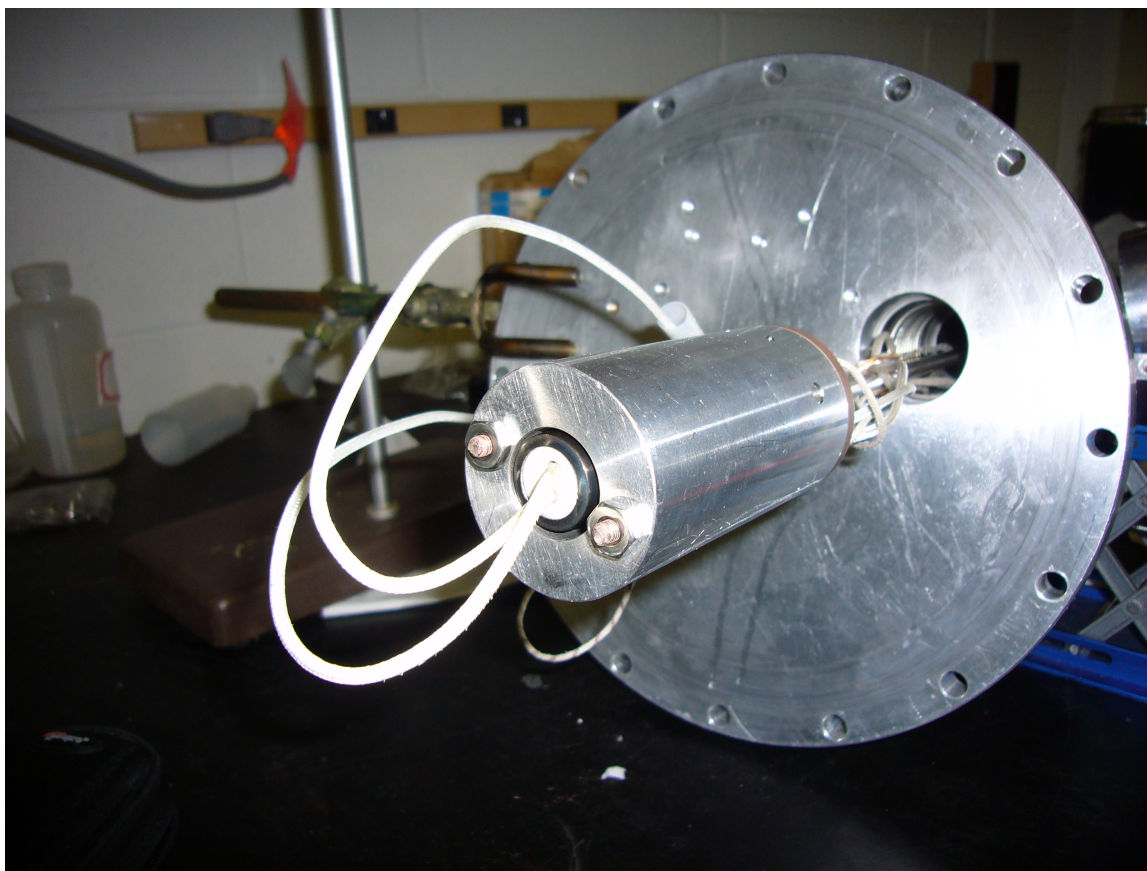


Figure 2.2: The second stage oven source

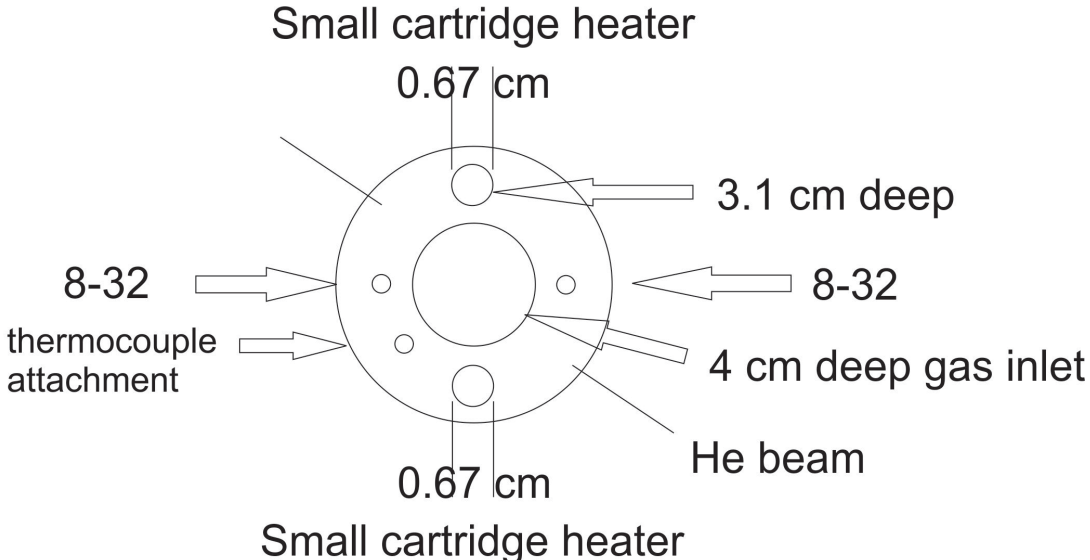
2.2 Evolution of the design of a two-stage oven source

In order to ensure that NAGMA was kept at a stable thermal equilibrium, a two-stage variable temperature source was designed using the CorelDRAW™ graphics suite. The first stage of the oven source is held at a constant temperature to vaporize NAGMA, while the second stage of the oven source is varied to control the temperature at which the equilibrium distribution of NAGMA is recorded. The pickup cell is an aluminum cylinder that is heated by one large cartridge heater and two small cartridge heaters connected in series. There is a port built into the aluminum block in which a thermocouple is secured with set screws. A cylindrical depression was drilled into the block so that the NAGMA molecules can come into thermal equilibrium at the

temperature of the aluminum block. A cross section of this depression was bored out, allowing the droplet beam to pick up NAGMA. In order to be certain the molecules of NAGMA were in thermal equilibrium with the aluminum block, copper mesh was tightly packed into the depression, leaving only enough space for the droplet beam to pass through. Therefore, the NAGMA molecules have a high probability of undergoing multiple collisions with copper that is at the same temperature as the aluminum block. Schematics of the aluminum block are shown in Figures 2.3 and 2.4. The pickup cell remained unchanged throughout the design process.

All holes are clearance holes

Front



Back

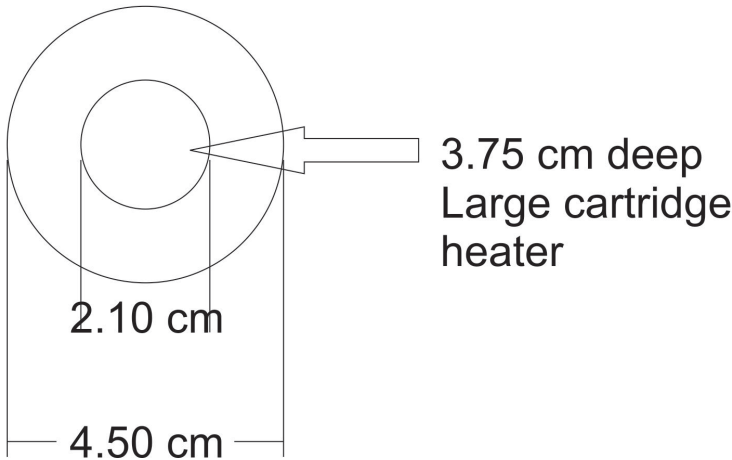


Figure 2.3: View of the front and back faces of the aluminum block

Key:
SC: set screw 4-40
CH: clearance hole 8-32

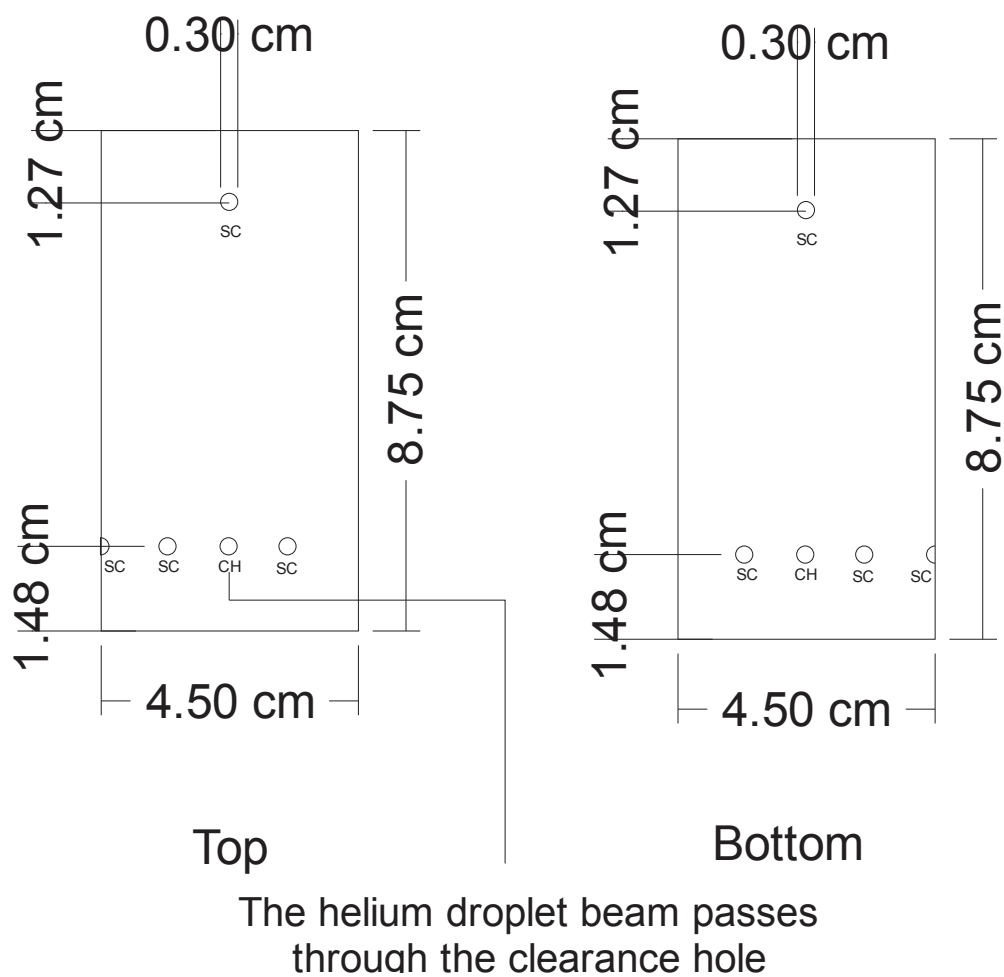


Figure 2.4: Lengthwise views of the aluminum block

Although the design of the pickup cell remained unchanged throughout the testing process, the molecular source was changed multiple times. In its first iteration, the source was temperature stabilized using two nested round bottom glass bulbs (Figure 2.5).



Figure 2.5: Biomolecule source

The inner bulb held NAGMA and was kept under vacuum. The port into which NAGMA was introduced into the inner bulb was sealed with an O-ring that tightened around a glass plug. The inner bulb ended in a stainless steel stem to which a Cajon O-ring compression fitting could be attached. The outer bulb was a three-stem glass bulb. The middle stem formed a junction between the outer and inner bulbs. The other two stems were for the introduction of a solvent and the attachment of a condenser to reflux the solvent. Problems with this design arose because it was difficult to completely warm the inner bulb. The glass plug extended into the inner bulb and could not be heated, which created a cold spot where NAGMA would collect. The glass plug was modified to a stainless steel pipe in the hope that it could be closed with a metal seal that could be

resistively heated using heat tape. However, the part of the glass stem connecting the outer bulb to the inner bulb was also a cold spot, and we came to the conclusion that the nested glass bulb design was not effective.

As an alternative to the nested glass bulb design, a Swagelok cap was filled with NAGMA and directly attached to the metal tube for its introduction into the pickup cell. A thermocouple was attached to the cap and the temperature was monitored over time while it was heated with heat tape. The temperature monitoring program demonstrated that once the sample holder reached thermal equilibrium, the temperature was stable to 0.2 °C over an hour. A copper pipe originally connected the biomolecule source through a vacuum feedthrough, ending in the pickup cell. Copper was chosen for its thermal conductivity so that no cold spots would form in the pipe. However, copper was too soft to support the weight of the aluminum block and sagged over time. A stainless steel tube was introduced instead, but formed a cold spot on the vacuum side of the tube feedthrough. This was remedied by insulating a nichrome wire and resistively heating it. This prevented the vacuum feedthrough from acting as a heat sink and the biomolecules were able to travel into the pickup cell without condensing on the transfer tubes.

2.3 NI LabVIEW™ temperature stabilization program

LabVIEW™ (Laboratory Virtual Instrument Engineering Workbench) is a graphical programming language produced by National Instruments designed for data acquisition. In order to ensure the temperature stability of the aluminum block, a temperature stabilization program was written that can communicate with the dc power supply. The user can apply a certain voltage step and time step in order to control the voltage ramp rate. The program monitors a temperature reading from the thermocouple

connected to the aluminum block to decide if the voltage should be ramped up or down. The finest voltage adjustment possible using a GW Instek PST-3202 is 0.01 V. After testing the temperature stabilization of the aluminum block under vacuum, it was determined that once the block reaches thermal equilibrium its temperature only fluctuates by < 0.2 °C over the ten minutes it takes to record each infrared spectrum because of the mass of the aluminum block. Therefore, the temperature stabilization program was not essential for this experiment.

2.4 Mass spectrometer detection

As discussed in section 1.4, the ion depletion signal is derived from vibrational excitation of the helium nanodroplet by the IR-OPO laser, which is discussed in the following section (2.5). The helium droplet beam enters the pick-up cell to pick up the model dipeptide. The doped helium nanodroplets then enter into an off-axis mass spectrometer. The laser output beam is counter-propagated to the helium nanodroplet beam. Figure 2.6²⁸ shows the orientation of the mass spectrometer in relationship to the helium beam and laser excitation source.

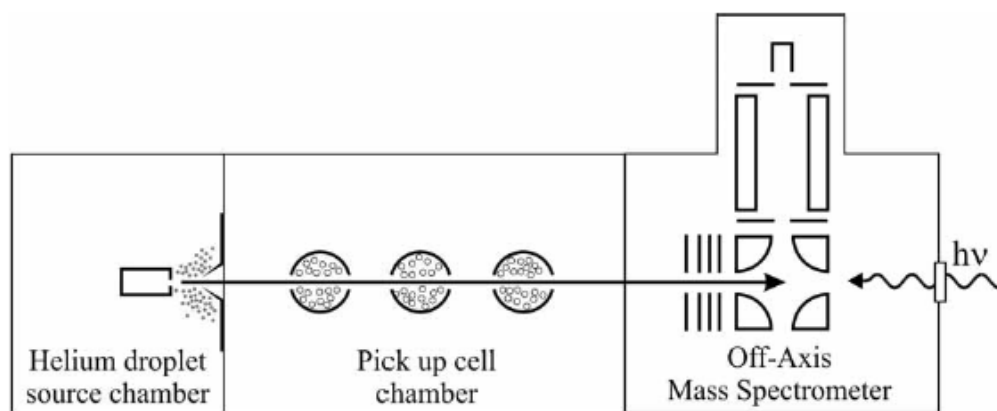


Figure 2.6: The HENDI experimental design

For the VTMA measurements discussed in Section 1.4, this experimental design is augmented to include a laser multipass region, shown below in Figure 2.7.³⁰

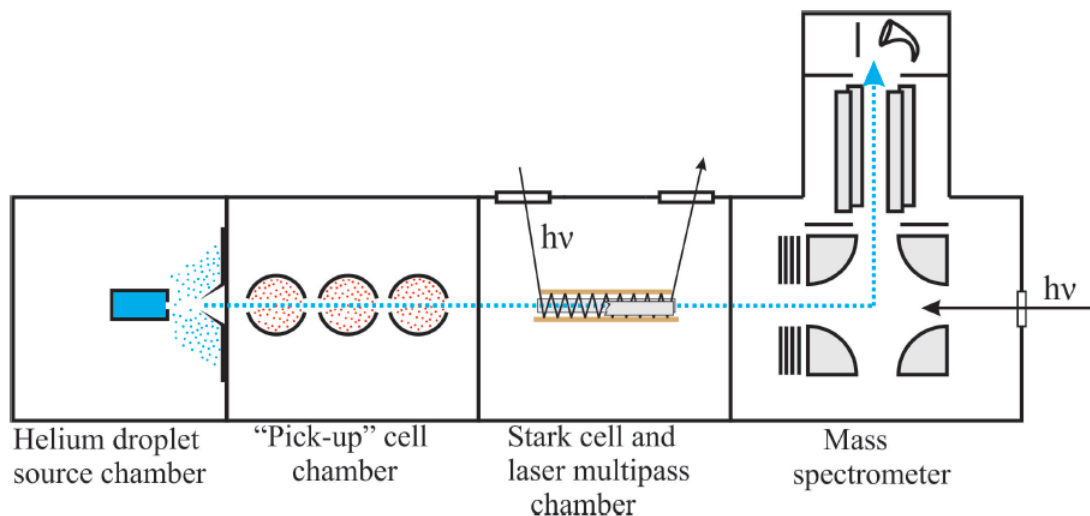


Figure 2.7: The HENDI setup including the Stark cell

Electron impact ionizes a helium atom, and subsequent charge hopping occurs, leading to the formation of ionized helium clusters. Below is the mass spectrum of a neat helium beam, where there are no solvated species. Each peak in the mass spectrum is associated with a He_n^+ cluster, and therefore the peaks are separated by 4 amu.

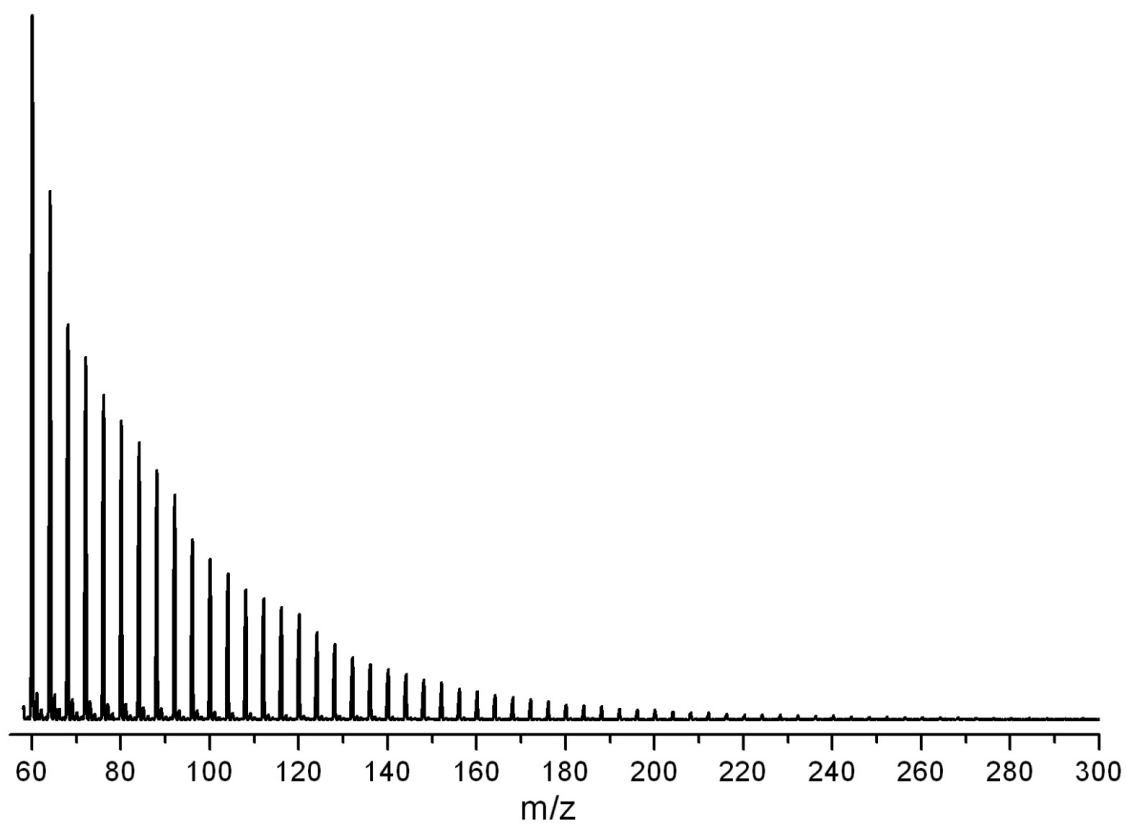


Figure 2.8³⁰: Neat helium droplet mass spectrum

There are two ways in which to operate the Extrel quadrupole mass spectrometer, either radio frequency (rf)-only mode or in a fixed dc voltage mode. When the mass spectrometer is operated in rf-only mode, all masses are allowed to pass to the detector. When the dc voltage on the quadrupole is fixed, the transmission of ions that contribute to a single mass to charge ratio is allowed. The equation which governs the potential applied to the quadrupole is shown below.

$$f(t) = U + V\cos(2\pi ft)$$

In the above equation, U is the dc voltage and V is the peak amplitude of a radio frequency voltage at the frequency f. In order to run the spectrometer in rf-only mode, U

is set to zero. U is varied to create the mass filter. The detector used is a conversion dynode multiplier, and the power supply controller is the Extrel model 5221.

Optically Selected Mass Spectra (OSMS) are obtained for NAGMA. This is accomplished by fixing the frequency of the IR-OPO laser on an N-H stretch transition of NAGMA and obtaining a mass spectrum. The OPO is amplitude modulated, therefore the OSMS corresponds to the difference in the mass spectrum with and without the OPO excitation.³⁰ In this way it is ensured that the OSMS represents the mass spectrum of only the droplets that have molecular species excited by the IR laser.

2.5 Infrared laser interrogation of conformer distributions in helium nanodroplets

The laser used for vibrational excitation is a singly-resonant, continuous wave Infrared Optical Parametric Oscillator (IR-OPO) produced by Lockheed Martin Aculight (ARGOS 2400-SF-15). A singly resonant OPO is one in which only the signal wave is resonated. Its advantages are they have much higher output powers, better stability, and a greater ease of alignment and tuning than doubly or triple resonant lasers. As seen in Figures 2.6 and 2.7 above, the laser beam is counter-propagated to the helium nanodroplet beam through a window in the mass spectrometer. The excitation beam of the laser is the tunable idler output which has a range of 2.2-4.6 μm .

A schematic of the cw-SR-OPO system is shown in Figure 2.9 below.

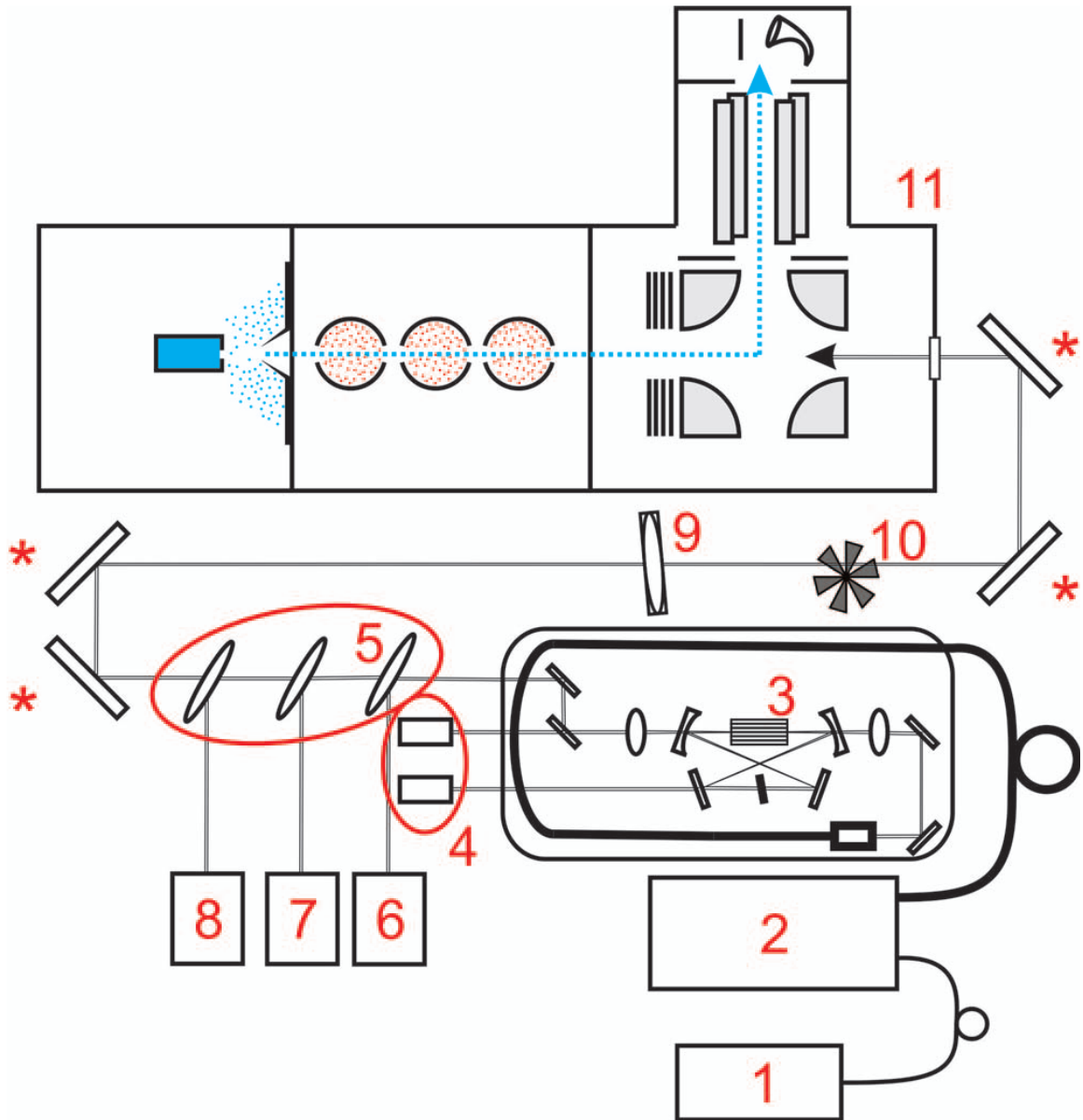


Figure 2.9: Experimental setup of the cw-SR-OPO coupled to a HENDI spectrometer³¹

For the above figure, the numbers correspond to (1) the seed laser, (2) diode-pumped fiber amplifier, (3) cw-SR-OPO, (4) beam dumps for the pump and signal beams, (5) CaF₂ beam splitters, (6) power meter, (7) wavemeter, (8) Fabry-Perot scanning etalon, (9) Glan-Taylor polarizer, (10) optical chopper, and lastly (11) the HENDI spectrometer. There are three tuning elements that work in concert to scan the frequency ranges needed: the translation of a fan-out PPLN crystal, the rotation of an

intracavity etalon, and the tuning of the pump seed laser wavelength via piezoelectric strain.³¹ These three elements work together to tune the laser over a range of several hundred wavenumbers. For our experiment, the OPO is scanned over a range of only $\sim 10 \text{ cm}^{-1}$ in order to measure the N-H nonbonded spectral bands for the two conformers, which both lie within the $3490\text{-}3500 \text{ cm}^{-1}$ region. A saturation study showed that a polarizer was necessary to attenuate the output of the idler beam to $\sim 200 \text{ mW}$. The lock-in amplifier has a 3 second time constant; therefore, it takes thirty seconds to scan over the full width half max of each peak, which corresponds to $\sim 15 \text{ GHz}$ (0.5 cm^{-1}).

CHAPTER 3

THE ENTHALPY OF INTERCONVERSION OF NAGMA

3.1 Mass spectra of NAGMA

The first step in determining the interconversion enthalpy of NAGMA is to dope helium nanodroplets with the dipeptide. The full mass spectrum of NAGMA is shown below in Figure 3.1. This spectrum includes NAGMA fragments, helium droplet fragments, and any impurities in the HENDI system. However, this does not tell us which peaks come specifically from NAGMA fragmentation. To determine this, an OSMS (Laser OFF-ON) mass spectrum must be measured.

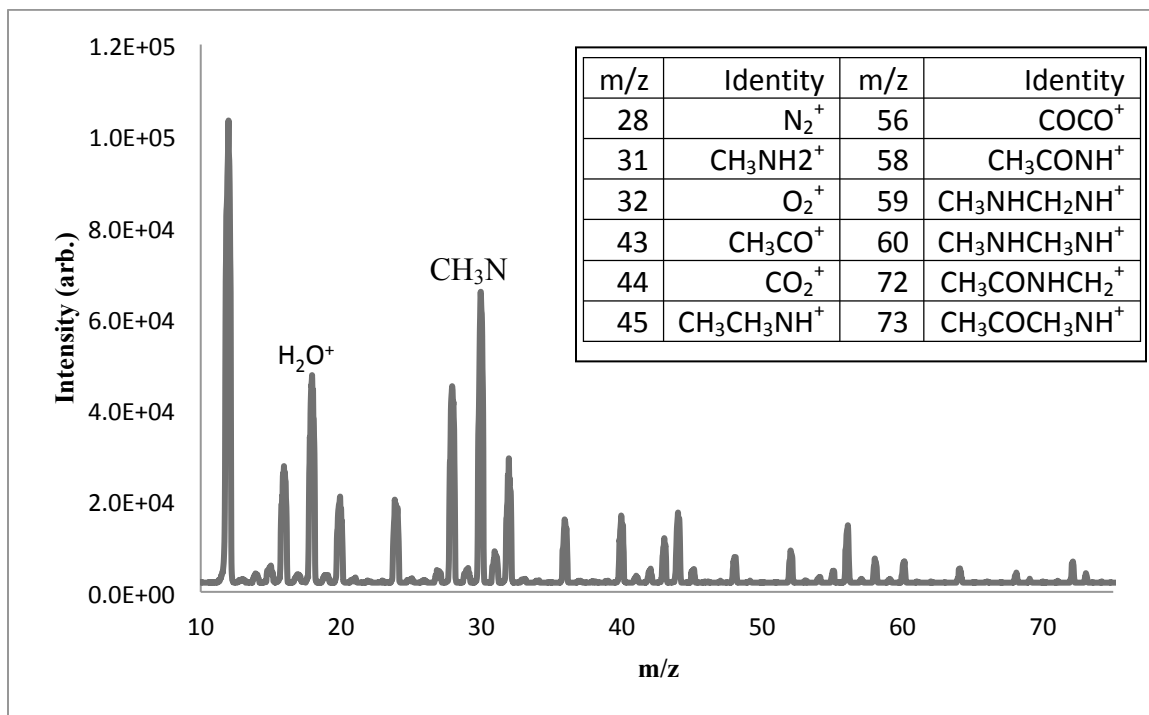


Figure 3.1: The mass spectrum of NAGMA scanned from $m/z = 10-75$

To determine exactly which peaks are contributed to by fragments of NAGMA, an OSMS was scanned. The following figure shows the optically selected mass spectrum of the two NAGMA conformers by recording the mass spectrum of NAGMA while probing the N-H stretches centered around 3497.1 and 3494.7 cm^{-1} , shown in Figure 3.2 below.

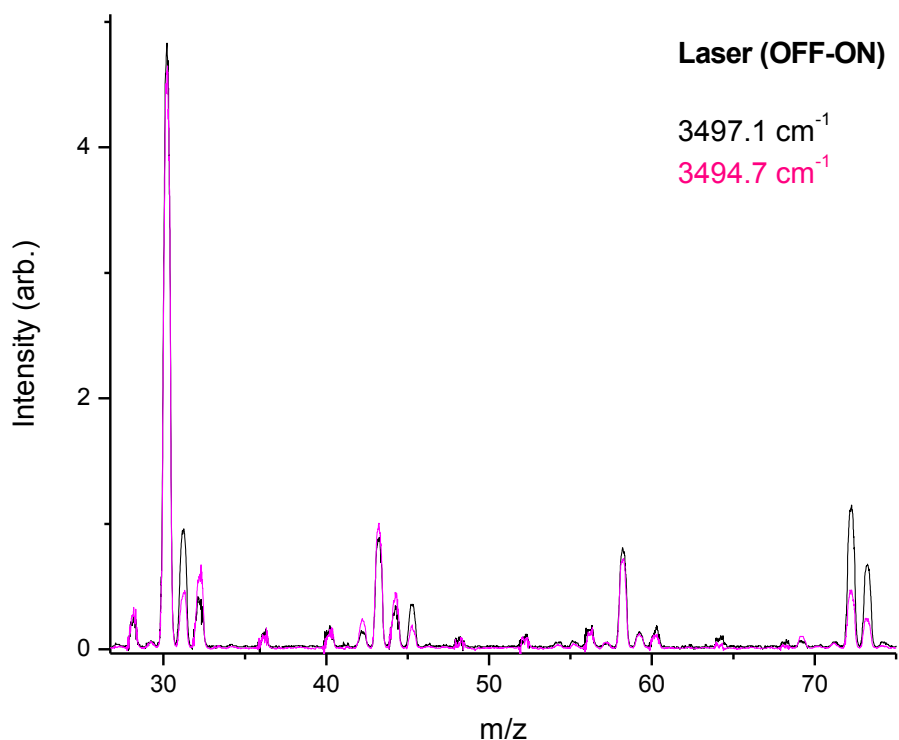


Figure 3.2: OSMS of N-H stretches studied

By observing the OSMS above, it is clear that the mass at 30 m/z (CH_3NH^+) is the most intense, and therefore that is the mass channel that the depletion signal is taken from for this experiment.

3.2 Infrared spectroscopy of NAGMA

To determine the relative energetics of the two low-energy conformers of NAGMA, a survey scan of the N-H stretch region of the infrared spectrum was measured, as shown in Figure 3.3. This spectrum contains two low-frequency hydrogen-bonded N-H stretches and two high-frequency nonbonded N-H stretches. The nonbonded N-H stretches in the 3490-3500 cm^{-1} region were compared at several different pick-up cell temperatures to generate the van't Hoff plot.

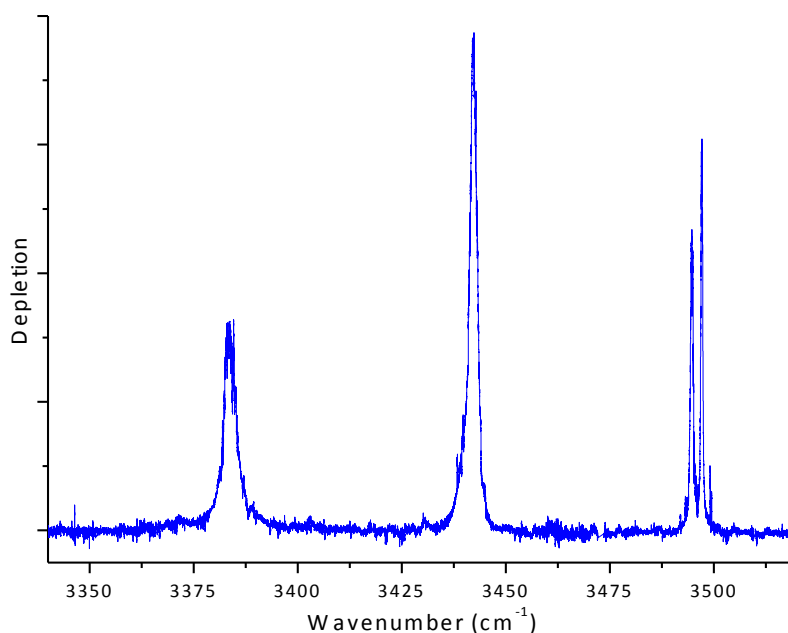


Figure 3.3: Survey scan of NAGMA

Shown below in Figure 3.4 is a close-up view of the 3490-3500 cm^{-1} region of the spectrum, which corresponds to the nonbonded N-H stretch region. The green lines show the Lorentzian lineshapes that were applied to the peaks in order to determine their areas. There are two Lorentzian lines that are fitted to the lower frequency band. This was done to give the best possible fit to the data. It seems that the lower frequency band has a more Gaussian lineshape, while the higher frequency band is more Lorentzian. The reasoning behind this is not well understood at this time. However, we have ruled out overlapping

transitions due to conformers or higher order clusters via careful vapor pressure dependent studies. The non-Lorentzian shaped peak seems to be due to a free N-H stretch of a single conformer, as determined from the VTMA analysis, similar to the higher frequency Lorentzian band.

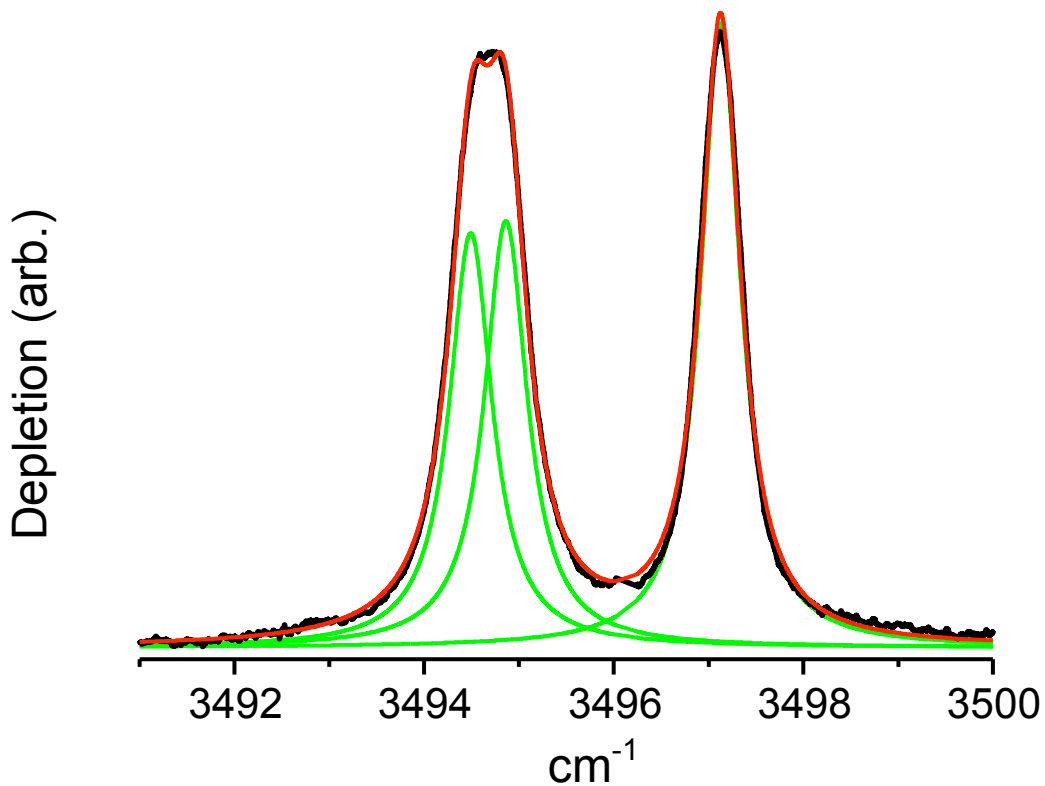


Figure 3.4: An expanded view of the N-H nonbonded stretches of the C5 and C7 conformers

3.3 Assignments of the two conformers of NAGMA to spectra

The conformer geometry assignments are determined by comparing the computed VTMA for the nonbonded N-H stretches of the C5 and C7 conformers to the experimental values. The computations were carried out using the rotational constants and the permanent dipole moments determined at the MP2/aug-cc-pVTZ level of theory.

The value of α is then varied until agreement with the experimental measurements is achieved. In Figures 3.5 and 3.6 below, calculations of five different values of α are compared to the experimental VTMA, shown in the black trace. It was determined that the free N-H stretch of C5 has a calculated $\alpha = 70^\circ$ with a μ_p of 3.38 D and rotational constants of $A = 0.169 \text{ cm}^{-1}$, $B = 0.0228 \text{ cm}^{-1}$, and $C = 0.0203 \text{ cm}^{-1}$ and the free N-H stretch of C7 has a calculated $\alpha = 78^\circ$ with a μ_p of 3.08 D and rotational constants of $A = 0.0937 \text{ cm}^{-1}$, $B = 0.0337 \text{ cm}^{-1}$, and $C = 0.0283 \text{ cm}^{-1}$. These values of α agree quite well with the experimental VTMA's associated with the lower and higher frequency bands, respectively. This indicates that the 3494.7 and 3497.1 cm^{-1} bands should be assigned to C5 and C7, respectively.

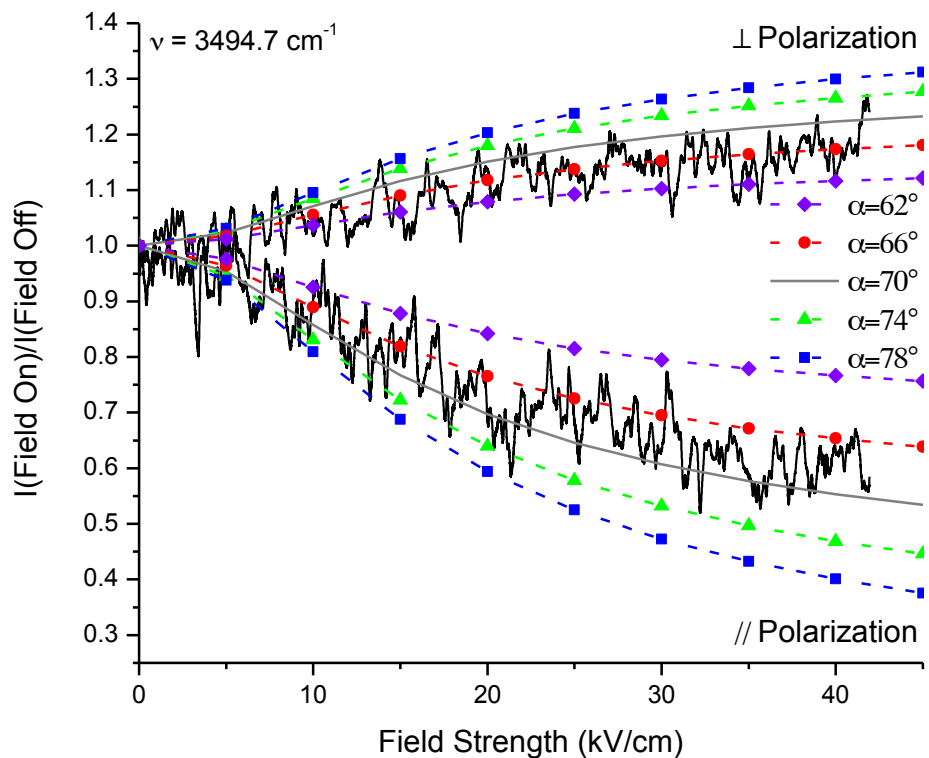


Figure 3.5: The experimental and calculated VTMA's at the MP2/def2-TZVPD level of theory for the C5 conformer. The solid line corresponds to the simulation using the computed VTMA for the free N-H stretch of the C5 conformer, namely 70° .

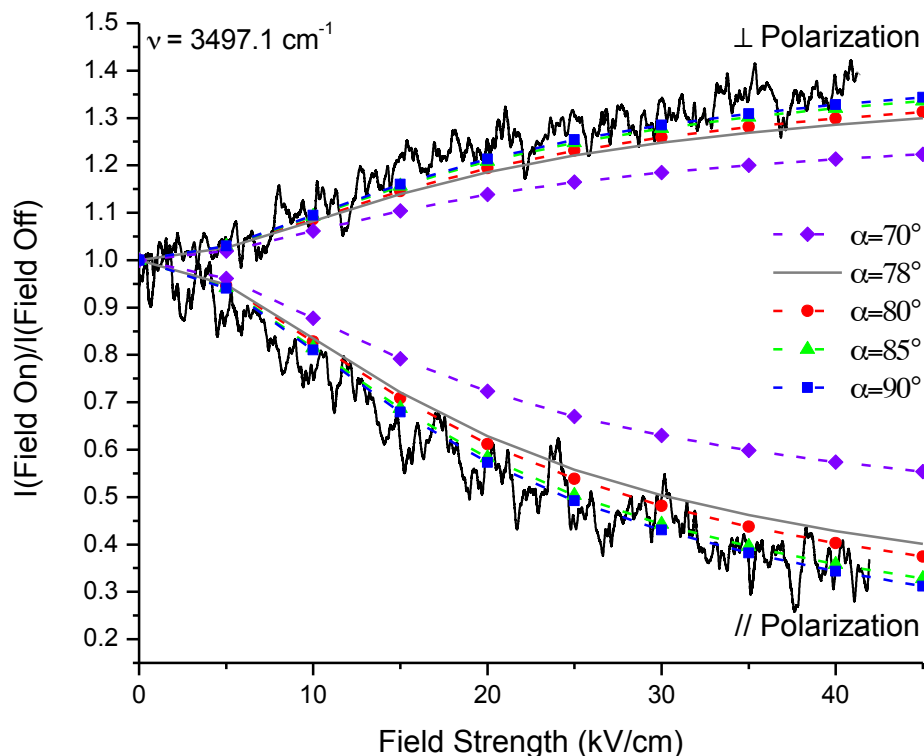


Figure 3.6: The experimental and calculated VTMA at the MP2/def2-TZVPD level of theory for the C7 conformer. The solid line corresponds to the simulation using the computed VTMA for the free N-H stretch of the C7 conformer, namely 78° .

By cross referencing the optimized geometries of both the C5 and C7 conformers with the VTMA of the conformers, their spectral frequencies are assigned. Because the VTMA belonging to the C5 conformer were probed at 3494.7 cm^{-1} and the ones belonging to the C7 conformer were probed at 3497.1 cm^{-1} , their spectral signatures are definitively assigned.

3.4 Enthalpy of interconversion from the van't Hoff plot

Now that the two free N-H stretch bands have been assigned to the two low energy NAGMA conformers, C5 and C7, a van't Hoff plot of the enthalpy of

interconversion of C5↔C7 can be determined. An experimental van't Hoff plot was generated by taking the natural log of the ratio of the integrated areas for the two non-bonded N-H stretch bands and plotting them against the inverse of the Kelvin temperature at which they were measured, as shown below in Figure 3.7. Error bars on individual data points are associated with the 2σ deviation of triplicate measurements for each temperature setting. From the experimental van't Hoff plot it was determined that $\Delta H^\circ = -4.52 \pm 0.12$ kJ/mol, i.e. the C5 conformer is higher in enthalpy than the C7 conformer by 4.52 ± 0.12 kJ/mol.

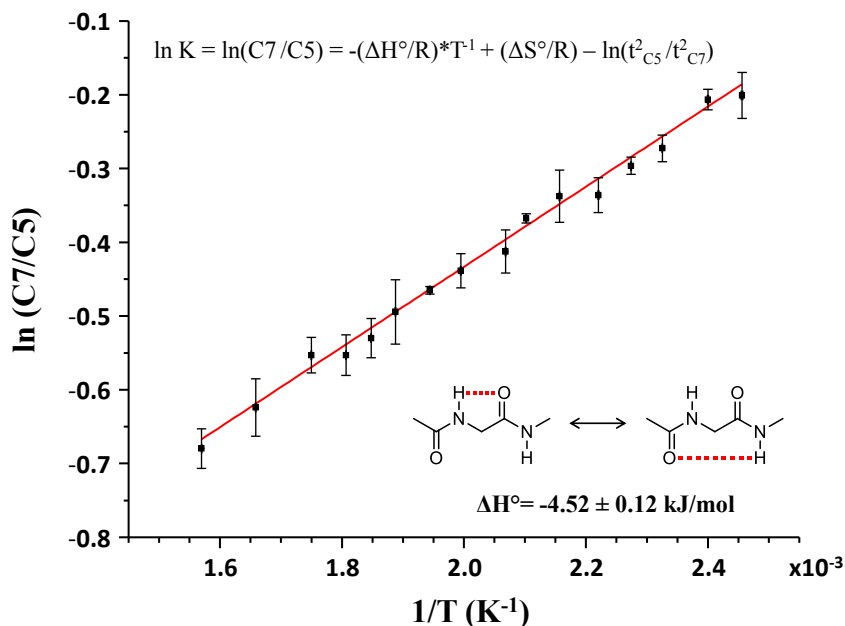


Figure 3.7: The van't Hoff plot of the interconversion of C5↔C7

The theoretical calculations for the interconversion enthalpy of NAGMA conformers (C5↔C7) are tabulated in Figure 3.8 below.

Method	ΔH (kJ/mol)
PBEPBE	-1
B3LYP	0.7
cam-B3LYP	1
M06-2x	-0.7
MP2	-4.2
MP2/aug-cc-pVTZ	-4.4

Figure 3.8: DFT and ab initio calculations of the enthalpy of interconversion of NAGMA ($C5 \leftrightarrow C7$). All methods use the def2/TZVPD basis set unless otherwise stated.

As shown in the table, there is significant scatter in the calculated enthalpy of interconversion; however it is generally within 4 kJ/mol of the experimental value. It is clear from this table that the error from these calculations is much larger than the error of the experimental value (± 0.12 kJ/mol). Therefore, this is a benchmark experiment with much greater accuracy than can be attained using theoretical methods.

CHAPTER 4

CONCLUSIONS AND FUTURE PROJECTS

The two-stage oven source design has been proven to keep a constant vapor pressure of biomolecule in the pick-up cell as well as control the voltage applied to cartridge heaters to be able to shift the conformer distributions over a broad temperature range. This source will be used in subsequent studies of this type where large molecules are probed. Such experiments are discussed later in the chapter. The temperature stabilization program developed was not useful for this experiment because the aluminum block did not change its temperature very quickly over time; therefore temperature stabilization was not necessary. However, the program does work and can be utilized in future experiments if needed.

The onset of zwitterion formation of peptides solvated with water is another problem of high interest in biophysical science. Amino acid chains are neutral in the gas phase, but with subsequent addition of water molecules they form zwitterions. It is currently unknown in the literature exactly the number of water molecules it takes to form the zwitterionic form of peptide chains, although theory has predicted that it takes two water molecules.³² The two-stage oven source can be used in tandem with a second pick-up cell that introduces water into the chamber. By varying the vapor pressure of water introduced into the pick-up cell, the probability of the pick-up of a certain number of water molecules into the NAGMA solvated helium nanodroplet can be controlled.

The assignment of the low-energy conformers of NAGMA to the spectrum was obtained using their vibrational transition moment angles. Because the free N-H stretches of the C5 and C7 conformers of NAGMA are so close in energy, ab initio frequency calculations are not accurate enough to assign their correct frequencies. VTMA's are used instead because the permanent dipole is a more accurate and stronger indicator for conformer assignment than frequency calculations. The calculated VTMA of $\alpha = 78^\circ$ for the C7 conformer does not have as ideal agreement with the experimental VTMA as the C5 conformer. In future work, the permanent dipole moment of the C7 conformer will be increased in the VTMA calculation in order to determine the best possible fit to the experimental data. The use of VTMA's to determine structural characteristics can also be applied to larger peptide chains to determine the secondary structural characteristics of peptides of increasing scale.

By taking the natural log of the integrated area of the C5 conformer divided by the integrated area of the C7 conformer and relating it to the inverse of the Kelvin temperature at which each peak was scanned, a van't Hoff plot was created, from which the experimental enthalpy of interconversion of C5 \leftrightarrow C7 was determined. The enthalpy of interconversion of C5 \leftrightarrow C7 is experimentally determined to be $\Delta H^\circ = -4.52 \pm 0.12$ kJ/mol. This method can also be applied to the determination of the enthalpy of interconversion for other large biomolecules, such as dipeptides, larger peptide chains, and nucleic acid base tautomers, such as guanine and cytosine.

REFERENCES

- (1) Jager, M.; Zhang, Y.; Bieschke, J.; Nguyen, H.; Dendle, M.; Bowman, M. E.; Noel, J. P.; Gruebele, M.; Kelly, J. W. *Proc. Natl. Acad. Sci. U. S. A.* **2006**, *103*, 10648.
- (2) Ramabhadran, R. O.; Sengupta, A.; Raghavachari, K. *J. Phys. Chem. A* **2013**, *117*, 4973.
- (3) Xie, Y.; III, H. F. S.; Silaghi-Dumitrescu, R.; Peng, B.; Li, Q.-s.; Stearns, J. A.; Rizzo, T. R. *Chem. Eur. J.* **2012**, *18*, 12941.
- (4) Yan, B. X.; Sun, Y. Q. *J. Biol. Chem.* **1997**, *272*, 3190.
- (5) Boopathi, S.; Kolandaivel, P. *J. Biomol. Struct. Dyn.* **2012**, *31*, 158.
- (6) Gorbunov, R. D.; Stock, G. *Chem. Phys. Lett.* **2007**, *437*, 272.
- (7) Gorbunov, R. D.; Kosov, D. S.; Stock, G. *J. Chem. Phys.* **2005**, *122*, 1.
- (8) Brauner, J. W.; Flach, C. R.; Mendelsohn, R. *J. Am. Chem. Soc.* **2005**, *127*, 100.
- (9) Dian, B. C.; Longarte, A.; Winter, P. R.; Zwier, T. S. *J. Chem. Phys.* **2003**, *120*, 133.
- (10) Dian, B. C.; Longarte, A.; Mercier, S.; Evans, D. A.; Wales, D. J.; Zwier, T. S. *J. Chem. Phys.* **2002**, *117*, 10688.
- (11) Pohl, G.; Perczel, A.; Vass, E.; Magyarfalvi, G.; Tarczay, G. *Phys. Chem. Chem. Phys.* **2007**, *9*, 4698.
- (12) Wang, J.; Chen, J.; Hochstrasser, R. M. *J. Phys. Chem. B* **2006**, *110*, 7545.
- (13) Oomens, J.; Steill, J. D.; Redlich, B. *J. Am. Chem. Soc.* **2008**, *131*, 4310.

- (14) Puzzarini, C.; Biczysko, M.; Barone, V.; Largo, L.; Pena, I.; Cabezas, C.; Alonso, J. L. *J. Phys. Chem. Lett.* **2014**, *5*, 534.
- (15) Kapota, C.; Ohanessian, G. *Phys. Chem. Chem. Phys.* **2005**, *7*, 3744.
- (16) Polfer, N. C.; Oomens, J.; Dunbar, R. C. *Chem. Phys. Chem.* **2008**, *9*, 579.
- (17) Silva, M. A. V. R. d.; Silva, M. d. D. M. C. R. d.; Santos, A. F. L. O. M.; Juaristi, E. *J. Phys. Chem. B* **2011**, *115*, 9401.
- (18) Ramabhadran, R. O.; Sengupta, A.; Raghavachari, K. *J. Phys. Chem. A* **2013**, *117*, 4973.
- (19) Brauns, E. B.; Dyer, R. B. *Biophys. J.* **2005**, *89*, 3523.
- (20) Brust, R.; Lukacs, A.; Haigney, A.; Addison, K.; Gil, A.; Towrie, M.; Clark, I. P.; Greetham, G. M.; Tonge, P. J.; Meech, S. R. *J. Am. Chem. Soc.* **2013**, *135*, 16168.
- (21) Mukherjee, P.; Kass, I.; Arkin, I. T.; Zanni, M. T. *Proc. Natl. Acad. Sci. U. S. A.* **2006**, *103*, 3528.
- (22) Yan, B. X.; Sun, Y. Q. *J. Biol. Chem.* **1996**, *272*, 3190.
- (23) Stearns, J. A.; Seaiby, C.; Boyarkin, O. V.; Rizzo, T. R. *Phys. Chem. Chem. Phys.* **2009**, *11*, 125.
- (24) Potts, A. R.; Baer, T. *J. Phys. Chem.* **1998**, *108*, 869.
- (25) Harris, D. C.; Bertolucci, M. D. *Symmetry and Spectroscopy: An Introduction to Vibrational and Electronic Spectroscopy*; Oxford University Press: New York City, 1978.
- (26) Brink, D. M.; Stringari, S. *Z. Phys. D: At., Mol. Clusters* **1990**, *15*, 257.
- (27) Skvortsov, D. S.; Vilesov, A. F. *J. Chem. Phys.* **2009**, *130*, 1.

- (28) Choi, M. Y.; Douberly, G. E.; Falconer, T. M.; Lewis, W. K.; Lindsay, C. M.; Merritt, J. M.; Stiles, P. L.; Miller, R. E. *Int. Rev. Phys. Chem.* **2010**, *25*, 15.
- (29) Dong, F.; Miller, R. E. *Science* **2002**, *298*, 1227.
- (30) Morrison, A. M. Master's Thesis, The University of Georgia, 2012.
- (31) Morrison, A. M.; Liang, T.; Douberly, G. E. *Rev. Sci. Instrum.* **2013**, *84*, 1.
- (32) Jensen, J. H.; Gordon, M. S. *J. Am. Chem. Soc.* **1995**, *117*, 8159.